Test Structures for Stepwise Deformation Sensing on Super-flexible Strain Sensors

Test Structures for Stepwise Deformation Sensing on Super-flexible Strain Sensors

C. Wang [1], B. B. Xu [1], J.G. Terry [2], S. Smith [2], A.J. Walton [2], Y. Li [1]
[1]Smart Materials and Surfaces Lab, Faculty of Engineering and Environment,
Northumbria University, Newcastle upon Tyne, NE1 8ST, UK
Email: yifan.li@northumbria.ac.uk
ben.xu@northumbria.ac.uk
[2]SMC, Institute for Integrated Micro and Nano Systems
School of Engineering, the University of Edinburgh, Edinburgh, EH9 3JF, UK

***Abstract* — Developing MEMS sensors with a high strain sensing range (up to 0.6) and a stepwise sensing mechanism could enable widespread downstream applications, by allowing intimate, mechanically conformable integration with soft biological tissues. Most approaches to date focus on challenges to associate the sensing mechanism with high peak strains under large deformation.**

By designing and characterizing test structures with multi-switching electrodes on super-flexible substrates, this research has established a strategy for stepwise strain-sensing mechanism based on elastic instabilities. The growing and co-existence of wrinkles and creases on multiple electrodes with different dimensions are observed under lateral strains ranging between 0.3 and 0.6. Initial electrical measurements of the multi-switching mechanism has been demonstrated with a two stage resistance value change observed under changing compressive strain. Further investigation will focus on the device optimization and mechano-electrical signal processing.

I. Background

Flexible electronic and MEMS devices have become one of the more interesting technologies for next generation applications such as bio-medical electronics, flexible circuits, sensors and actuators [1-4]. Recent development has shown that elastic substrates have great potential to withstand high strain deformation during bending, compressing and stretching, when complying with local features such as metal interconnects and integrated transducers [5-8].

Among recently developed flexible MEMS applications, a versatile set of approaches exploits the sensing and actuation of planar compression strain achieved by triggering the elastic instabilities with placing pre-strain in an elastomer mounting substrate [9-11]. This paper presents a concept in which elastomeric substrates with engineered distributions of a set of materials and structural characteristics yield stepwise strain sensing of in-plane deformations. The related technologies and newly developed sensing mechanism could shed a light on the future applications in tunable optics and stretchable electronics.

II. Methodology

Test structures with a single switching mechanism to sense super-flexible strain have been reported [4, 8]. These devices operate by a pair of finger electrodes contacting as a result of surface creasing generated in the gap at the critical strain. At this point the measured resistance of these device switches from open (~10^{13} Ω) to closed (~10^{2} Ω). The critical strain values are of course related to the dimensions of the designed gap between the finger electrodes along the compression axis [8].

Such mechano-electrical response (strain - resistance) test structures can be employed for super-flexible substrate strain sensing. However, each device performs as a digital sensor with "ON/OFF" logic, therefore only measuring a single critical strain value [8].

In order to increase the number of critical strain values the test structures can deliver without increasing the pad count, this paper focuses on studying the deformation behaviour of a test structure with multi-switching electrodes on super-flexible substrates. The ultimate target is to enable a multi-switching mechanism where the strain value can be determined by measuring the resistance of the test structures. The following characterisation will be focused on electrode geometry design related to the surface deformation (optical measurement), and electrical signal (resistance) as a function of strain change.

A. Test Structure Design

Figure 1 shows the test structures used, with the deformation study focusing using two different layouts:

- A two-terminal structure with four pairs of "finger" electrodes labelled F1 (longest) to F4 (shortest) making up the multi-switching strain sensing gate
- A four-terminal structure with a similar finger arrangement to that in design I

The original lengths of finger electrodes ($L_f = L_{f0}$ in figure 1) range from 225 to 265µm and 500µm to 525µm, with electrode widths either 20µm or 50µm. The gap between the finger electrodes L_g ranged between 5 and 95µm. The probe pads were all 500 µm x 500 µm (original length $L_e = L_{e0}$ = 500 µm) in size.

978-1-4673-XXXX-X/17 $XX.XX

These test structures are designed to enable both 2-point and 4-point Kelvin measurement of device resistance. The test structures are fabricated on stretched substrates and as the tension is reduces, the finger electrodes F1 to F4 will be brought into contact sequentially due to their different L_g values [4, 8]. The finger resistance values and any contact resistance can then be measured.

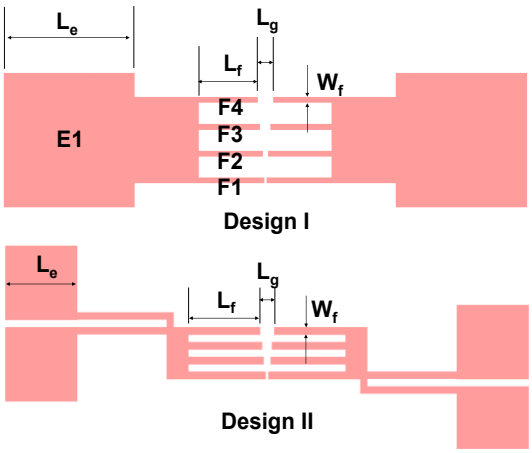

Fig. 1. Design layouts of the multi-switching high-strain sensing test structures.

B. *Fabrication Process*

The fabrication process involves the patterning of a gold layer on a silicon substrate and then transferring the pattern onto a pre-tensioned flexible substrate. The gold layer was patterned with a lift-off process using MEGAPOSIT™ SPR™ 220-7 positive photoresist. This involved depositing Au layers (with thickness ranging between ~16nm and ~100nm) on a silicon wafer with an anti-stiction SAM layer Perfluoro-decyl-trichloro-silane (FDTS, deposited using a MemsStar AURIX™ system). Alternatively, a thin C_4F_8 passivation layer deposited by Plasmatherm® Inductively Coupled Plasma (ICP) system could also be employed as an anti-stiction layer.

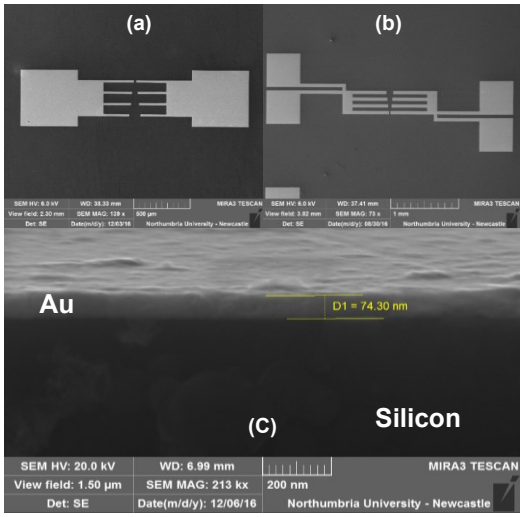

Fig. 2. SEM images showing (a) and (b) top view of the Au multi-switching test structures on silicon substrate, and (c) cross-sectional view showing Au thickness.

Fig. 2(a) and (b) shows SEM images (Tescan® Mira3) of the multi-switching electrode designs on silicon, with Fig2(c) showing a cross-section of the gold layer with a thickness of 74nm. With the test structure geometric designs reported above, the resistance of the fingers would be expected to vary between ~25 to 175 Ω for the reported gold film thicknesses.

With the gold now patterned the next stage is to transfer it onto the PDMS bi-layer. This bi-layer elastomer, consists of a thick and stiff mounting layer (3 mm thick, 9 mm width and 30 mm length) made of Vinylpolysiloxane, which was prefabricated and placed in a mechanical vice and pre-stretched from 5mm to 30mm length, before a softer unstressed thin PDMS bilayer (~110.13 µm thick) was attached.

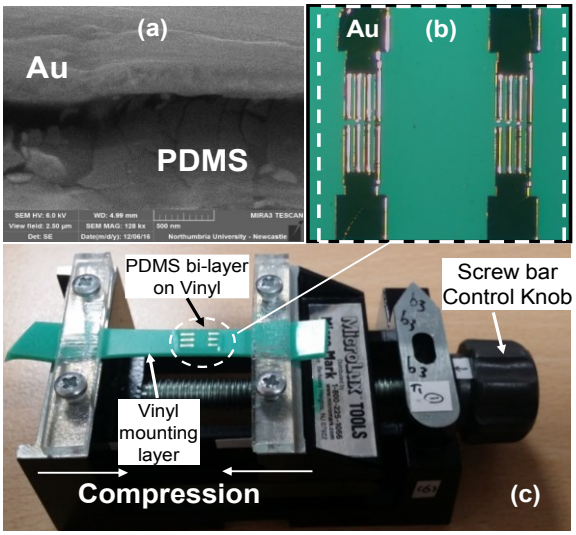

Fig. 3. (a) SEM images showing transferred Au sitting on PDMS bilayer (~110 µm thick), (b) microscopic top view of the transferred Au test structures on PDMS, and (c) photo of the entire device tensioned in the mechanical vice.

To transfer the Au electrodes they were treated with MPTMS (3-Mercaptopropyl-trimethoxysilane) as an SAM adhesive, by soaking in 25mM MPTMS in absolute ethanol solution for 3 hours. The electrodes were then transferred to the bi-layer elastomer flexible substrate (shown in Fig. 3) from the silicon carrier wafer using the dual SAMs stamping method reported in [4, 8].

C. *Strain testing set-up*

Figure 3(c) shows the completed devices in their jig with the Au - PDMS test structures, mounted on the Vinylpolysiloxane (green coloured) stiff layer under tensile stress (mechanically pre-stretched). The PDMS bilayer with the Au test structures (figure 3b) was then compressed by relaxing the pre-stretched Vinylpolysiloxane mounting layer controlled by turning the screw thread (pitch = ~ 1.25mm/turn) of the mechanical vice.

By relaxing the pre-stretched Vinylpolysiloxane mounting layer from L_0 to L, the PDMS bi-layer is compressed. Hence, the PDMS surface instabilities would be expected to change (Wrinkles-Creases) depending on the strain under uniaxial compression, which is given by:

$$\varepsilon = (L_0\text{-}L)/L_0 \qquad (1)$$

III. Measurements and Results

A. Optical measurement of Electrode Deformation

To quantitatively study the electrode deformation, compression strains were calculated before and during the formation of crease in the gap between electrodes by measuring the "L_{f0} and L_f" of the 4 finger electrodes, and "L_{e0} and L_e" of the contact electrodes. These results can then be compared with the mounting layer or substrate strain ε given by Eq. 1 which acts as a reference.

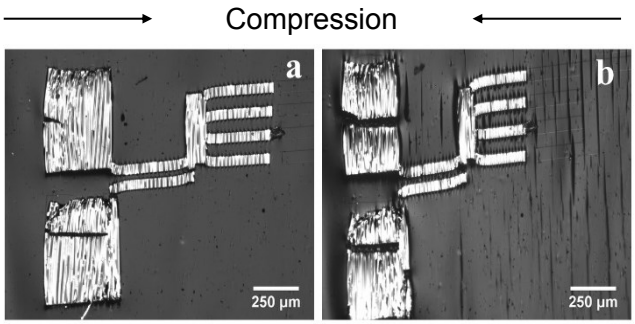

Fig. 4. Time sequential microscopic images showing the compression process generating creases (b) on PDMS and wrinkles on Au electrodes

As a result of the surface instability growth, Au electrodes on the PDMS surface may endure a different strain change to the PDMS bi-layer and the Vinylpolysiloxane mounting layers. Hence, 2-D measurements of the electrode deformation were undertaken using ImageJ software on photos taken using a Nikon® Eclipse LV100 microscope. The lengths were measured to determine the compression strain on Au electrodes of the multi-switching test structures during the compression process (fig. 4).

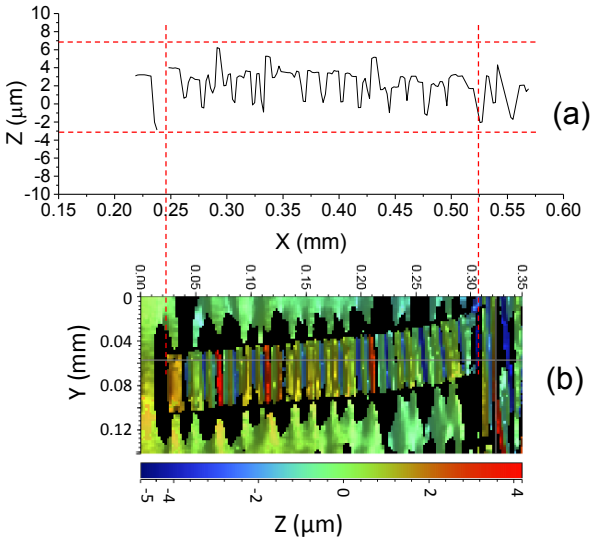

Fig, 5. Bruker GTK surface scan providing surface profile of F2 electrode shows both wrinkles on Au and creases on PDMS as (a) cross-section view, and (b) 2D contour top view

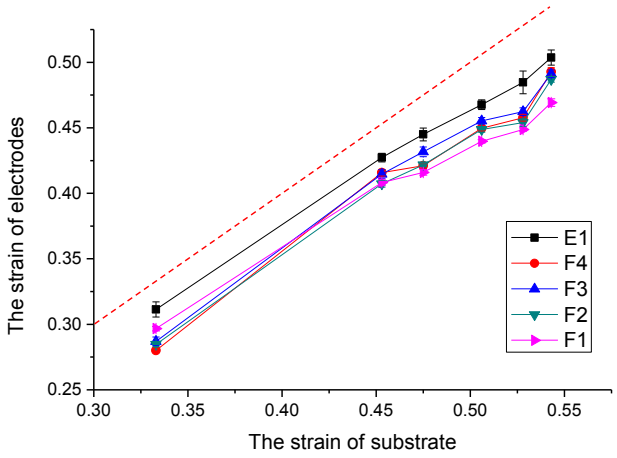

Fig. 6. Strain change comparison on multi-switching Au electrodes – finger electrodes F1 to F4, and contact pads E1. Red dotted line indicates the substrate strain change as a reference.

Figure 5 shows a surface deformation profile of the Au electrode test structures measured using a Bruker® GTK interferometry surface profiler. In addition to the length information, the amplitude of wrinkles (figure 5(a)) can also be observed during the process.

While Au wrinkling was observed at lower strain levels in a similar manner to previous reported single-switching test structures, the multi-switching structures have shown some interesting behaviour.

Details recorded in Fig. 4 and 5 show that, when creases start to form at strains $\varepsilon > 0.45$ on the PDMS surfaces, the compression ratios $(L_{f0} - L_f) / L_f$ start to lag behind the substrate strain change as shown in Fig. 6. This is more obvious on the finger electrodes (F1 to F4) than the probe pad (E1).

As a result, the multi-switching structures (especially the finger electrodes) are largely undamaged along the uniaxial compression direction, which makes electrical measurement of the multi-switching mechanism promising.

B. Electrical measurement of the Multi-switching mechanism

When there is a large strain change of up to 0.6 or 60%, it is inevitable that tensile transverse strains are generated by the uniaxial compressive strain change. Such tensile strain is usually perpendicular to the compression direction, and has been observed to cause damage to some parts of the test structure.

Figure 7(a) shows that the tensile strain changes on finger electrodes F1 to F4 are considerably larger than on the probe pads E1. This non-uniform strain distribution causes undesirable shear force to be generated on interconnects between the contact pads (E1) and (F1 and F4) in both design I and II. Figure 7(b) shows that on design II, right-angled interconnects also suffered damage due to similar shear forces.

This damage has resulted in the following compromises during the electrical testing:

1. Only 2-point resistance measurements were conducted at this stage.

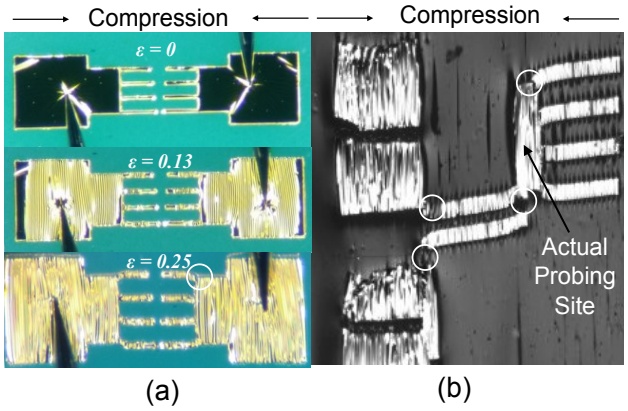

Fig. 7. Tensile strain perpendicular to the compression direction generated during strain increase on both (a) design I (probe tips present) and (b) design II. The damaged interconnects are highlighted by white circles.

2. The actual probing site of design II is as indicated in figure 7(b).
3. Only finger electrodes F2 and F3 were successfully involved in the multi-switching strain sensing.

However, despite the above issues, multi-switching with a large strain sensing mechanism has been achieved. Figure 8 shows the resistance measurements performed using an Everbeing EB8 manual probe station (with EB-05 probes) connected to a Keithley® 4200 analyzer (-1V to +1V sweep, with 0.2V/step). It should be noted that probing these devices is complicated by the wrinkling and creasing of the gold as well as the flexible and soft nature of the substrate membrane.

Figure 9 shows the resistance values of the test structure as a function of strain for design II shown in Figure 1. Each point is measured for a range of current level by sweeping between -1V and +1V, with 0.2V/steps. For this structure the designed L_g values for F2 and F3 finger electrodes were 12 µm and 21 µm respectively, with L_f = 509 µm and 518 µm, and W_f = 50 µm. Given the Au thickness in this case was around 70 nm, then the estimated finger electrode resistance would be in the region of 50 Ω. Therefore when the F2 electrodes are in contact, the calculated resistance of the test structure will be 100 Ω, assuming the contact resistance is zero. This will be reduced to

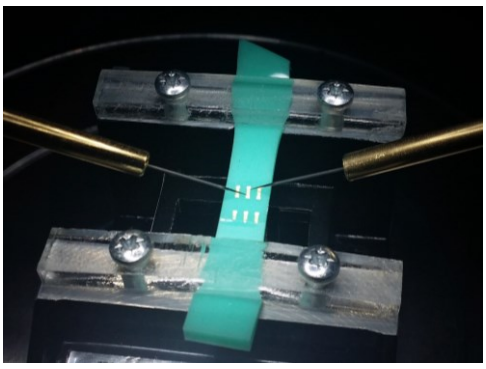

Fig. 8. Photo shows resistance measurements performed using an Everbeing EB8 manual probe station

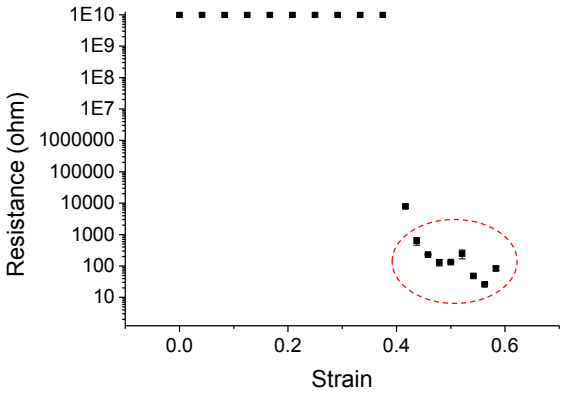

Fig. 9. Resistance of the test structure (design II, L_g) as a function of strain. The resistance change during the two-stage switching are highlighted in a red ring and detailed in figure 10.

50 Ω when F3 electrodes are also connected due to a higher strain.

From figure 10, it can be observed that the first switching stage happens at ε_s = 0.45, strain range 0.45 < ε < 0.52 with a resistance of ~120 Ω. The second switching stage occurs at ε_s = 0.54, strain range 0.54 < ε < 0.58 with the measured resistance being ~ 50 Ω. Note the error bars indicate multiple measurements at different current levels that in most cases indicate that Joule heating is not influencing the measurement. It is thought that the large variability in just the two data points is related to the contact resistance just before a good contact is achieved.

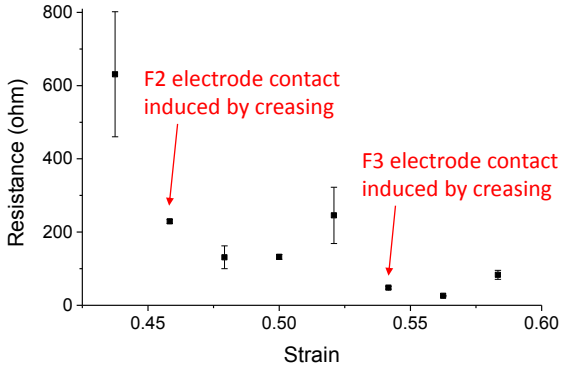

Fig. 10. Two-stage resistance switching strain sensing: Resistance of the test structure (design II, Lg) as a function of strain during the two-stage switching period (0.45< ε <0.52, and 0.54< ε <0.6).

The "switch on" strain ε_s results from the multi-switching test structure seem different to the previous reported values of single switching test structures with L_g = 12 µm and 21 µm reported in [8], which are 0.22 and 0.42 respectively and further investigation is required.

IV. Conclusions and Discussions

Test structures with the ability to detect multiple strain values on a super-flexible substrate have been designed, fabricated and

characterised, both optically and electrically. In contrast to the previously reported single switching test structures, multiple resistance values were generated at different switching strains on an individual device. This has been demonstrated using the multiple finger electrode test structure with different distances between the electrodes (the gaps are aligned along the compression axis).

During characterization, issues related to unwanted tensile strain perpendicular to the compression axis have been observed, which resulted in unexpected damage to the test structure interconnects. Future work will have to address minimizing such damage by layout modifications. The switching strain values of the multi-switching test structures related to the gap distances were observed to be different than values reported for the single switching devices and further investigation is required to compare the performance of the two structures.

ACKNOWLEDGMENT

This work is supported by EPSRC (EP/N007921/1, EP/L026899/1), and the royal society (RG150662). The authors would like to thank Everbeing who donated the probing system used in this work, and memsstar for providing the SAM coating facility. Data associated with this paper is available via Northumbria Research Data Management scheme: https://www.northumbria.ac.uk/research/research-data-management/

REFERENCES

[1] D.-H. Kim, et al., "Epidermal Electronics", Science, Vol. 333, pp. 838-843, 2011.

[2] W. Wu , X. Wen , and Z. L. Wang , "Taxel-Addressable Matrix of Vertical-Nanowire Piezotronic Transistors for Active and Adaptive Tactile Imaging", Science, Vol. 340 , pp. 952-957, 2013.

[3] D.-H. Kim , et al., "Stretchable and Foldable Silicon Integrated Circuits", Science, Vol. 320, pp. 507-511, 2008 .

[4] B.B. Xu , D. Chen , and R. C. Hayward, "Mechanically Gated Electrical Switches by Creasing of Patterned Metal/Elastomer Bilayer Films", Advanced Materials, Vol. 26, pp. 4381-4385, 2014.

[5] D. Y. Khang, H. Q. Jiang, Y. Huang, and J. A. Rogers, "A Stretchable Form of Single-Crystal Silicon for High-Performance Electronics on Rubber Substrates", Science, Vol. 311, pp. 208-212, 2006.

[6] D. Y. Khang, J. A. Rogers, and H. H. Lee, "Mechanical Buckling: Mechanics, Metrology, and Stretchable Electronics", Advanced Functional Materials, Vol. 19, pp. 1526-1536, 2009.

[7] M. S. White, et al., "Ultrathin, highly flexible and stretchable PLEDs", Nature Photonics, Vol. 7, pp. 811-816, 2013.

[8] Y. Li, J.G. Terry, S.Smith, A.J. Walton, G. McHale and B.B. Xu, "Elastic Instabilities Induced Large Surface Strain Sensing Structures (ElLS)", IEEE ICMTS, Tempe, AZ, USA, pp. 94-99, 2015.

[9] B.B. Xu, Q. Liu, Z. Suo, and R.C. Hayward, "Reversible Electrochemically Triggered Delamination Blistering of Hydrogel Films on Micropatterned Electrodes", Advanced Functional Materials, Vol. 26, pp. 3218-3225, 2016

[10] R. Xu et al., "Designing Thin, Ultrastretchable Electronics with Stacked Circuits and Elastomeric Encapsulation Materials", Advanced Functional Materials, published online, doi: 10.1002/adfm.201604545, 2017

[11] K. Nan et al., "Engineered Elastomer Substrates for Guided Assembly of Complex 3D Mesostructures by Spatially Nonuniform Compressive Buckling", Advanced Functional Materials, Vol. 27, p. 1604281, 2017